JOURNAL OF GEOPHYSICAL RESEARCH, VOL. 112, D15204, doi:10.1029/2007JD008530, 2007

Improved ground-based liquid water path retrievals using a combined infrared and microwave approach

D. D. Turner[1]

Received 11 February 2007; revised 14 May 2007; accepted 23 May 2007; published 4 August 2007.

[1] Radiative transfer modeling through cloudy atmospheres requires accurate measurement of the cloud properties. In liquid water clouds, accurate measurements of the liquid water path (LWP) are required, especially when the LWP is less than 100 g/m^2. A new ground-based retrieval algorithm was developed that retrieves LWP using infrared (8–13 μm and 3–4 μm) and microwave (23.8 and 31.4 GHz) radiance observations, as microwave radiance is sensitive to a large range of LWP (less than 5 to over 1000 g/m^2) and infrared radiance is extremely sensitive to LWP less than approximately 60 g/m^2. The random error in the retrieved LWP is estimated to be less than 4% when the LWP is less than 50 g/m^2 but, for larger LWPs, it increases to at least 12 g/m^2. The algorithm is also able to retrieve effective radius (r_e) when the LWP is less than approximately 60 g/m^2. This new retrieval algorithm was applied to data collected by the Atmospheric Radiation Measurement (ARM) program's Mobile Facility at Pt. Reyes, California, from July to August 2005. Daytime retrieved r_e values agree well to airborne in situ observations, with a mean bias of 0.11 μm. A radiative transfer model utilizing the retrieved cloud properties was used to compute the surface and top of the atmosphere fluxes. The flux residuals (observed minus calculated) demonstrate a significant reduction in scatter (approximately a factor of 2 for LWP < 40 g/m^2) relative to flux calculations where the cloud properties were determined by the microwave-only retrieval algorithm MWRRET.

Citation: Turner, D. D. (2007), Improved ground-based liquid water path retrievals using a combined infrared and microwave approach, *J. Geophys. Res.*, *112*, D15204, doi:10.1029/2007JD008530.

1. Introduction

[2] Accurate modeling the solar and infrared radiative flux though the atmosphere is critical for global climate models (GCMs) [e.g., *Cess et al.*, 1996], since it is the distribution of radiative and latent heating within the atmosphere that drives the atmospheric circulation [*Stephens*, 2005]. Improving the treatment of the interaction of clouds and radiation in GCMs is critical to improve the long-term predictive capability of GCMs. The U.S. Department of Energy's Atmospheric Radiation Measurement (ARM) program's overarching goal is to improve the radiative transfer parameterizations in GCMs, and especially in cloudy atmospheres [*Stokes and Schwartz*, 1994; *Ackerman and Stokes*, 2003]. In order to improve these parameterizations, ARM has equipped its ground-based climate research facilities with a wide variety of sensors to measure (directly or indirectly) the various geophysical variables that are critical to evaluate these radiative transfer models. These variables include the radiative fluxes themselves, profiles of atmospheric state (i.e., temperature and water vapor profiles), aerosol profiles, and importantly cloud macrophysical and microphysical properties.

[3] Cloud properties, including phase, water content, particle size distribution, and in the case of ice particles shape information can in principle be determined with in situ observations on airborne platforms. However, in situ observations suffer from several shortcomings, including small sample sizes, limited duration, and potential contamination due to the sampling approach. Therefore, while aircraft observations are very useful for characterizing cloud processes and provide one way to validate remote sensing techniques, these observations are not well suited for long-term cloud measurements for a climate research program.

[4] The approach adopted by the ARM program, and other programs such as CloudNet [*Illingsworth et al.*, 2007], is to deploy well-characterized remote sensors at ground-based sites that measure variables related to the actual geophysical quantities desired, and invert these observations to get the desired product. During the last decade, many different approaches were developed to retrieve the properties of liquid water clouds [e.g., *Min and Harrison*, 1996; *Liljegren and Lesht*, 1996; *Frisch et al.*, 1995; *Matrosov et al.*, 2004; *Donovan and van Lammeren*, 2001]. However, a recent study by *Turner et al.* [2007b] evaluated 18 of these algorithms for a "simple" single-layer, stratiform, warm-cloud case at the ARM Southern Great Plains (SGP) site

[1]Space Science and Engineering Center, University of Wisconsin-Madison, Madison, Wisconsin, USA.

0148-0227/07/2007JD008530$09.00

where the LWP was less than approximately 100 g/m^2. The resulting spread among the algorithms was as large as 40 g/m^2 or about 50% of the value. Therefore, while progress has been made in retrieving LWP and effective radius for liquid water clouds, more work is required to achieve the accuracies needed when the LWP is small.

[5] Radiative fluxes (both longwave and shortwave) are particularly sensitive to small perturbations in the LWP when the LWP was less than 100 g/m^2 [*Sengupta et al.*, 2003; *Turner et al.*, 2007b]. Recent studies have demonstrated that a large fraction of the liquid water clouds have LWP < 100 g/m^2 in different climate regimes, including the Arctic [*Shupe and Intrieri*, 2004], midlatitudes [*Marchand et al.*, 2003], and nonprecipitating clouds in the tropical western Pacific [*McFarlane and Evans*, 2004]. Therefore improving the retrieval of LWP, especially in scenes with small LWP, from ground-based observations is a high priority for climate studies.

[6] We have developed a new method that combines ground-based infrared and microwave radiance observations to retrieve LWP over the entire dynamic range of LWP, and also has excellent sensitivity to LWP when the LWP is small. We have applied this technique to data collected by the ARM Mobile Facility (AMF) [*Miller and Slingo*, 2007] at Pt. Reyes, California (38.092°N, −122.956°E) from July to August 2005. The algorithm is evaluated by using the retrieved cloud properties in a radiative transfer model to compute the surface shortwave and longwave downwelling radiative flux, and top-of-the-atmosphere (TOA) shortwave albedo. The comparison of these calculations with flux observations at the surface and at TOA demonstrates that the combined infrared+microwave method provides more accurate cloud properties than those derived from microwave radiometer (only) observations. The retrieval algorithm is also able to retrieve effective radius when the LWP is less than approximately 60 g/m^2; we have evaluated the retrieved effective radius using aircraft in situ observations collected at the AMF site.

2. Instruments

[7] Each ARM climate research facility, including the AMF, has a wide variety of in situ and remote sensing instrumentation, including state-of-the-art passive radiometers. In this study, we retrieve LWP and effective radius (r_e) using observations from the Atmospheric Emitted Radiance Interferometer (AERI) and the Microwave Radiometer (MWR), which are described below. The retrieval algorithm also needs ancillary information about the atmosphere. The cloud base height was determined from collocated Vaisala ceilometer observations, and atmospheric state information (i.e., temperature and water vapor profiles), as well as cloud temperature, is obtained from Vaisala RS92 radiosondes. Radiosondes were launched nominally every 6 hours during this AMF deployment. Each radiosonde moisture profile was scaled with a height-independent factor such that the integrated water vapor agreed with the precipitable water vapor (PWV) retrieved from the MWR [*Turner et al.*, 2003a]. This reduces the diurnal bias in the calibration of the radiosonde water vapor sensor.

2.1. AERI

[8] The AERI is a hardened, automated infrared interferometer that measures downwelling radiation from 530 to 3050 cm^{-1} (19.0 to 3.3 μm) with 1 cm^{-1} resolution [*Knuteson et al.*, 2004a, 2004b]. The AERI is built around a commercial interferometer and uses mercury cadmium telluride (MCT) and indium antimonide (InSb) detectors in a "sandwich" arrangement that provide good sensitivity to the downwelling infrared radiation. The AERI periodically views two well-characterized, high emissivity blackbodies, one of which is held at 60°C while the other floats at ambient temperature. An absolute calibration that is better than 1% of the ambient radiance (3-σ) is achieved through accurate monitoring of the blackbody temperatures (as well as the structural temperatures around the blackbodies) together with corrections for the instrument self-apodization and nonlinearity in the MCT detector [*Knuteson et al.*, 2004b]. The radiometric uncertainty of the AERI observations is determined from the imaginary portion of the calibration equation [*Knuteson et al.*, 2004b], and thus the scene-dependent instrument noise is determined directly for each AERI observation.

[9] Techniques that combine observations from multiple sensors must consider the differences in their temporal and spatial resolutions. The field-of-view of the AERI is 2.6 degrees (46 mrad) full-width half-maximum. The observation cycle utilized by the AERI at Pt. Reyes consisted of a 3-min average of sky radiance data, followed by 2-min views of each of the calibration blackbodies. This sampling strategy does not capture the (possibly large) variability in the cloud field as it advects over the instrument, but it does attain an excellent signal-to-noise ratio. The ARM program is currently modifying the AERI sampling strategy to increase the temporal resolution to provide 12-s average sky views every 30 s, and a principal component noise filter is being used to reduce the uncorrelated noise in these observations [*Turner et al.*, 2006].

2.2. MWR

[10] The ARM program has deployed two-channel MWRs at each of its facilities. These MWRs observe downwelling microwave radiance at 23.8 and 31.4 GHz. The former frequency is on the wing of the 22.2 GHz water vapor absorption line and the latter is in an atmospheric window where the signal is dominated by liquid water emission when there are clouds in the instrument's field of view. From these observations, statistical or physical retrievals can be used to retrieve both PWV and LWP [e.g., *Liljegren and Lesht*, 1996; *Turner et al.*, 2007a]. The instrument views a single blackbody target during each observation cycle. A noise diode, which inserts a fixed amount of additional energy, is switched on during the view of this target. This strategy results in essentially two blackbody views (i.e., with the noise diode off and on) and allows the gain of the instrument to be determined, provided the effective temperature of the noise diode is known. To calibrate the noise diode, tip-curve data [*Han et al.*, 1994] are collected during homogeneous clear-sky periods and an automated routine reduces these data to determine the gain of the system that is then used to calibrate the noise diode [*Liljegren*, 2000]. This procedure is able to maintain the calibration of the radiometer to

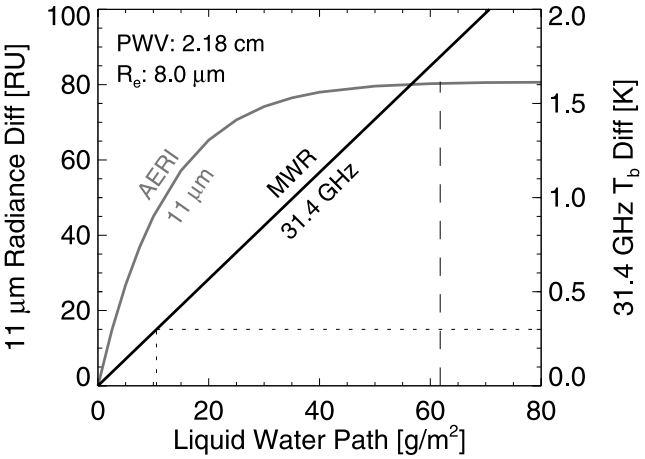

Figure 1. Simulated cloudy minus clear sky radiance difference at 11 μm and 31.4 GHz for a range of LWP. The radiometric uncertainty in the MWR observations at 31.4 GHz is approximately 0.3 K, which roughly translates into a 12 g/m^2 uncertainty in LWP (dotted line). However, since the sensitivity of the 31.4 GHz signal is linear with increasing LWP over this LWP range, MWR-based retrievals of LWP will have at least 12 g/m^2 uncertainty over this entire range. The uncertainty in the AERI observations is less than 1 RU at 11 μm (1 RU is 1 mW/(m^2 sr cm^{-1})), and thus the AERI has sensitivity to changes in LWP until the LWP increases above about 60 g/m^2 (dashed line), at which point the change of infrared radiance to changes in LWP decrease below the level of the AERI instrument uncertainty. The AERI's sensitivity to LWP is especially large for smaller LWP values. Both calculations use the same atmospheric configuration: the temperature and water vapor were observed at the ARM SGP site in October 1999, the PWV is 2.18 cm (a value close to the mean PWV seen at Pt. Reyes), the cloud base is at 1 km, the cloud is 300 m thick, and the effective radius is 8.0 μm.

approximately 0.3 K RMS [*Liljegren*, 2000]. The MWR uses the same antenna for both frequencies, and thus the field of view for each is slightly different (5.9° and 4.5° full-width half-maximum for 23.8 and 31.4 GHz, respectively). The instrument averages downwelling radiance for 1 s each for both channels (serially, not simultaneously) every 20 s. The remainder of the time in the 20-s period is spent viewing the blackbody and other housekeeping tasks.

3. Retrieval Algorithm

3.1. Sensitivity to LWP

[11] For over two decades, ground-based MWRs have been used to provide estimates of LWP. At 31.4 GHz, the downwelling radiance responds linearly with increasing LWP for LWP less than 100 g/m^2 (Figure 1). The radiometric uncertainty of the MWR observations at 31.4 GHz is approximately 0.3 K, and thus the uncertainty in the LWP retrievals is at least ±12 g/m^2 at any point in the LWP range (the dotted line in Figure 1). However, the MWR's LWP uncertainty is usually considered to be at least 25–30 g/m^2 because of uncertainties in the microwave absorption model or retrieval method employed [e.g., *Turner et al.*, 2007b; *Marchand et al.*, 2003; *Westwater et al.*, 2001; *Hewison et al.*, 2006]. Furthermore, recent studies have also shown that significant biases in the MWR observed radiance need to be accounted for to reduce the clear sky biases in LWP [*Turner et al.*, 2007a; *Gaussiat et al.*, 2007]. Therefore the LWP derived from the MWR has unacceptably large uncertainties when the LWP is less than 100 g/m^2, being 25% or more.

[12] The sensitivity to LWP by a ground-based infrared radiometer is significantly different than for a microwave radiometer. The radiometric uncertainty of the AERI observations at 11 μm is less than 1 mW/(m^2 sr cm^{-1}) (henceforth called a radiance unit RU) for typical midlatitude conditions. For LWP < 50 g/m^2, the sensitivity of the downwelling 11 μm radiance to changes in LWP are much greater than the AERI uncertainty. However, as the LWP increases, the downwelling infrared radiance saturates and reaches an asymptote at about 60 g/m^2, where the sensitivity of the downwelling 11 μm radiance to changes in LWP decreases to the level of the AERI instrument uncertainty (Figure 1).

[13] Therefore a ground-based infrared radiometer has good sensitivity to clouds with small LWP when the uncertainty in the MWR retrievals is relatively large; conversely, the infrared signal saturates at larger LWP amounts where the relative uncertainty in the MWR values is smaller. Our combined infrared-microwave retrieval algorithm takes advantage of these complementary sensitivities to provide more accurate retrievals of LWP.

3.2. Combined Infrared and Microwave Retrieval Algorithm

[14] The combined infrared-microwave retrieval algorithm is an extension of the Mixed-phase Cloud Retrieval Algorithm (MIXCRA) developed by *Turner* [2005]. MIXCRA was designed to retrieve the optical depth and effective radius of both the liquid and ice components in Arctic clouds from extended range AERI observations in the 8–13 μm and 18–24 μm bands. From the liquid water optical depth and effective radius, the LWP was computed. The algorithm utilizes an optimal estimation approach, and thus the uncertainties in the observations and the sensitivity of the forward model are propagated to provide uncertainties in the retrieved products. The capability of MIXCRA to retrieve properties of both the ice and liquid phases in mixed-phase clouds is limited to conditions where the 18–24 μm band is semitransparent. Because of the strong water vapor absorption in this band, this requires that the PWV be less than 1 cm. However, if a priori information on the cloud phase is known, this information can be used by the algorithm and enables it to retrieve the properties of the single-phase cloud. The algorithm is utilized in this manner to retrieve LWP and effective radius when the PWV is larger than 1 cm.

[15] However, the dynamic range of the retrieved optical depth in the early version of MIXCRA was limited to visible optical depths below approximately 6. At optical depths above this limit the emissivity in some portions of the 8–13 μm window is unity and thus the algorithm no longer has enough information to accurately retrieve effective radius. This was discussed by *Turner and Holz* [2005], who incorporated additional observations from the 3–4 μm band (also observed by the AERI) into the algorithm during the

Table 1. Spectral Channels Utilized in the MIXCRA Retrievals

Center Wavelength	Center Wavelength	Spectral Width
12.2 μm	820.0 cm^{-1}	6.0 cm^{-1}
11.1 μm	901.6 cm^{-1}	6.2 cm^{-1}
8.9 μm	1128.5 cm^{-1}	9.0 cm^{-1}
8.7 μm	1145.1 cm^{-1}	5.8 cm^{-1}
4.1 μm	2455.0 cm^{-1}	10.0 cm^{-1}
3.8 μm	2610.0 cm^{-1}	20.0 cm^{-1}
3.5 μm	2860.0 cm^{-1}	20.0 cm^{-1}
23.8 GHz	0.79 cm^{-1}	0.30 GHz
31.4 GHz	1.05 cm^{-1}	0.30 GHz

daytime as an additional constraint to improve the retrievals in these cases. This updated "2-band" version of MIXCRA could retrieve LWP, effective radius, and optical depth for all single-layer liquid clouds that had LWP below approximately 60 g/m^2 (the exact upper limit depends on the effective temperature of the cloud and the amount of water vapor between the instrument and the cloud).

[16] To obtain LWP across its entire dynamic range (i.e., less than 5 to over 1000 g/m^2), we have modified MIXCRA to be a "3-band" algorithm. The observed vector, **Y**, now includes both AERI (8–13 μm and 3–4 μm) and MWR (23.8 and 31.4 GHz) radiance observations, where the MWR observations were averaged over the AERI's sky averaging period. The spectral channels used in the retrieval are listed in Table 1. The forward model uses the LBLDIS model (which is a combination of the LBLRTM and DISORT [*Turner et al.*, 2003b]) for the infrared calculations and the MonoRTM model [*Clough et al.*, 2005; *Turner et al.*, 2007a] for the microwave calculations. The infrared and microwave gas absorption forward models share the same theoretical basis, as the MonoRTM is a monochromatic version of the LBLRTM. However, the liquid water aspects of the two models are different. The MonoRTM uses the liquid water absorption model of *Liebe et al.* [1991], but the scattering properties of the water drops used by LBLDIS are determined using Mie theory.

[17] For this study, the state vector that we are retrieving is $\mathbf{X} = [\tau, r_e, F_c]^T$, where τ is the optical depth of the liquid cloud [unitless], r_e is the effective radius of the droplets [μm], and F_c is the cloud fraction in the AERI's field of view during its averaging period [unitless] (the T denotes matrix transpose). The algorithm retrieves the extinction infrared optical depth τ_{IR}; however, this is converted to the "geometric-limit" optical depth τ by the relationship $\tau = 2/Q_{e,IR}\ \tau_{IR}$; from this point forward "optical depth" will always refer to the geometric-limit extinction optical depth. F_c is an effective cloud fraction, which allows the downwelling radiance I_{scene} to be modeled as

$$I_{scene} = F_c\ I_{cloudy} + (1 - F_c)\ I_{clear}. \tag{1}$$

Turner and Holz [2005] have shown that F_c is highly correlated with the true cloud fraction in the AERI's field of view.

[18] MIXCRA retrieves the state vector using a physical-iterative approach, where for iteration n+1, we derive $\mathbf{X}^{n+1}$ as

$$\mathbf{X}^{n+1} = \mathbf{X}_a + \left(\mathbf{S}_a^{-1} + \mathbf{K}^T\mathbf{S}_\varepsilon^{-1}\mathbf{K}\right)^{-1}\mathbf{K}^T\mathbf{S}_\varepsilon^{-1}(\mathbf{Y} - F(\mathbf{X}^n) + \mathbf{K}(\mathbf{X}^n - \mathbf{X}_a)), \tag{2}$$

where $\mathbf{X}_a$ is the a priori state vector with its covariance matrix $\mathbf{S}_a$, $\mathbf{S}_\varepsilon^{-1}$ is the covariance matrix of the observations, and $\mathbf{K}$ is the Jacobian of the forward model at $\mathbf{X}^n$. The Jacobian is computed using finite differences due to the nonlinearity of the infrared radiative transfer. The observation covariance matrix includes contributions from three sources: random instrument uncertainties, uncertainty in the PWV, and uncertainty in the cloud temperature. The first of these sources is assumed to be frequency-independent (i.e., no cross terms in the covariance matrix), but the last two are correlated with wavelength and thus $\mathbf{S}_\varepsilon^{-1}$ has off-diagonal entries [*Turner*, 2005]. The uncertainty in each AERI observation is derived from the imaginary part of the complex calibration equation [*Knuteson et al.*, 2004b], while the uncertainty in the PWV and cloud temperature was assumed to be 5% and 2 K, respectively.

[19] The optimal estimation approach used here allows the uncertainties in the observations and the a priori state vector to be propagated to provide uncertainties in the retrieved variables. The 1-σ uncertainties in the state vector **X** are given by $\mathbf{e}_x$, where

$$\mathbf{e}_x\mathbf{e}_x^T = \left(\mathbf{S}_a^{-1} + \mathbf{K}^T\mathbf{S}_\varepsilon^{-1}\mathbf{K}\right)^{-1}. \tag{3}$$

[20] The a priori state vector $\mathbf{X}_a$ and its covariance matrix $\mathbf{S}_a$ are often computed from climatology. However, if the data used to determine the climatology does not span all conditions then the a priori determined in this manner will be too restrictive and potentially bias the retrieved parameters. While in situ aircraft data from July 2005 above the Pt. Reyes site (discussed later) are available, these data were not used in the a priori state vector. Instead, we have arbitrarily chosen $\mathbf{X}_a$ to be $[8.0, 8.0, 0.9]^T$, but also assumed large uncertainties in these quantities (1-σ values of 10, 2.0, and 0.2, respectively) such that the a priori is not a serious constraint to the retrieval algorithm.

[21] MIXCRA does not retrieve LWP directly (i.e., LWP is not an element of the state vector **X**), rather it is derived from the retrieved optical depth and effective radius as

$$\mathrm{LWP} = \frac{2}{3}\rho_w r_e \tau, \tag{4}$$

where ρ_w is the density of liquid water and r_e is constant in the column. The uncertainties in r_e and τ are propagated to provide uncertainties in LWP. It should be noted that for large LWP, the infrared spectrum is totally opaque. For cases where the LWP is just above the saturation point for the infrared, the AERI observations continue to add information to the retrieval by requiring the retrieved LWP to be larger than the infrared saturation level. However, if the LWP is significantly larger than the saturation point, then the entire information content on LWP is coming from the MWR and the uncertainty in the derived LWP using this approach is virtually the same as in a physical-iterative retrieval that used only the MWR observations [e.g., *Turner et al.*, 2007a].

[22] An advantage of the optimal estimation approach is that we can easily determine the information content in the observations relative to a retrieved variable. One measure of the amount of information contained in the observations

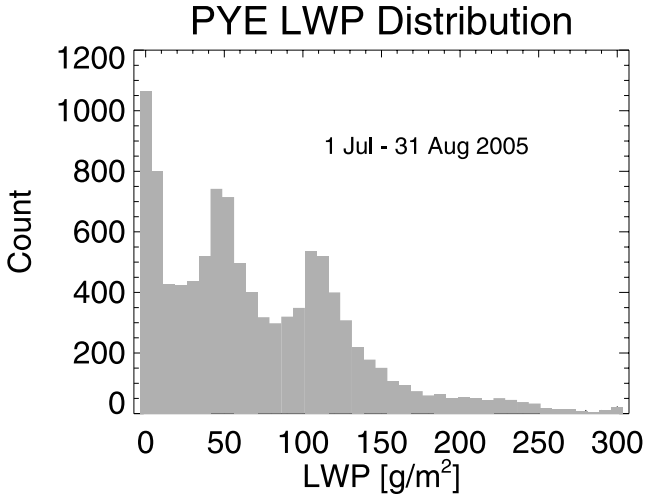

Figure 2. Distribution of LWP from MIXCRA for 1 July to 31 August 2005 over the AMF site at Pt. Reyes, California. There are 10,481 observations in this distribution. The first, second, and third quartile values are 25, 58, and 109 g/m^2, respectively.

about a retrieved variable is to compute the ratio of the uncertainty of the retrieved variable (computed using equation (3)) to the uncertainty of its a priori value. For example, for LWP < 50 g/m^2, the ratio of the uncertainty in the retrieved effective radius to the uncertainty in the a priori value of the effective radius (which was assumed to be 2 μm above) is less than 0.3; however, as the LWP increases beyond 60 g/m^2 this ratio increases dramatically toward the upper limit of 1. Large values of this ratio imply that the observation does not have much information about the retrieved parameter, which results in the a priori value having a larger weight in the retrieval of that parameter. This makes intuitive sense for the retrieval of r_e since the infrared spectrum is semitransparent for LWP < 60 g/m^2 (Figure 1) and thus the effective radius can be determined. When the infrared spectrum becomes opaque for LWP larger than this threshold, the retrieved r_e is being constrained only by the observations from the MWR that contain no information on particle size, and thus the r_e value returned by the retrieval algorithm will be a random variable from a Gaussian distribution with a mean and standard deviation specified by the assumed a priori value and its standard deviation (8 μm and 2 μm, respectively, for this work). Similarly, all of the information on the effective cloud fraction F_c is carried in the infrared spectrum. Therefore the subsequent analysis of r_e and F_c below are restricted to cases where the infrared spectrum is semitransparent.

4. Results

[23] The improved MIXCRA (infrared plus microwave) algorithm was applied to data collected by the AMF at Pt. Reyes, California, from July to August 2005. The AMF was deployed to this location to study the microphysical properties of the clouds and drizzle as the marine stratus clouds move onshore. During this 62-day (two-month) period, the ceilometer identified clouds overhead 89% of the time and their bases were always less than 500 m above the ground. The distribution of the MIXCRA-retrieved LWP is given in Figure 2. During this period, there were four short episodes of cirrus (a total of 3.7 days, which were identified using the outgoing longwave radiation measured by the Geostationary Operational Environmental Satellite (GOES-10)), that were removed from this analysis. The median value of the LWP distribution (retrieved using MIXCRA) is 58 g/m^2, with first and third quartile values of 25 and 109 g/m^2, respectively. Thus this is an excellent data set to test the accuracy and robustness of the improved MIXCRA algorithm relative to microwave-only retrieval algorithm for LWP < 100 g/m^2.

[24] Marine stratiform clouds, such as those observed at Pt. Reyes, occasionally will contain regions where the cloud is drizzling. *Gerber* [1996] demonstrated that marine stratocumulus clouds typically have two drizzle modes, a light mode where the liquid water content of the drizzle is less than 0.01 g/m^3 and a heavy mode where the liquid water content is significantly large than this threshold. Light mode drizzle does not affect the microwave retrievals of LWP [*Löhnert and Crewell*, 2003] or the infrared retrievals because of small amount of liquid in the drizzle droplets, and thus the MIXCRA-retrieved LWP is not affected. When the drizzle is in the heavy mode, the LWP is typically well above the infrared saturation point, and thus sensitivity of the MIXCRA-retrieved LWP to the drizzle is the same as sensitivity of a microwave-only retrieval of LWP in these cases [*Löhnert and Crewell*, 2003].

4.1. Uncertainties in LWP and r_e

[25] As indicated above, the MIXCRA algorithm provides the uncertainties in the retrieved parameters. We selected the cases where the MIXCRA algorithm successfully retrieved r_e, τ, and LWP in overcast conditions (F_c > 0.95) by screening the data where the 1-σ uncertainty in r_e was less than 1 μm and r_e < 15 μm. This resulted in 1420 nighttime cases and 1318 daytime cases. A case was considered to be "daytime" if the solar elevation was more than 8 degrees above the horizon, as for elevations below this limit the solar contribution in the 3–4 μm spectral region is not used in the MIXCRA retrieval; all other cases are considered to be "nighttime." The distributions of the uncertainty in LWP and r_e as a function of LWP are shown in Figure 3.

[26] The uncertainty in the retrieved r_e is smallest for cases where the LWP is approximately 10 g/m^2 (Figure 3), which coincides with the LWP range where the infrared radiance has the largest sensitivity to change in LWP (Figure 1). The random error in the retrieved r_e values is less than 0.2 μm for 1 g/m^2 < LWP < 30 g/m^2 and less than 0.4 μm for 30 g/m^2 < LWP < 50 g/m^2. The scatter in the 1-σ uncertainties in the retrieved r_e are similar for both daytime and nighttime retrievals, but there is a small amount of additional scatter in the daytime results. This additional variability is introduced by the utilization of the radiance observations in the 3–4 μm band and the solar scattered radiation that is detected and utilized by the retrieval; however, as we will discuss below, the use of this band in the retrieval removes a bias in the r_e retrievals.

[27] The uncertainty in the retrieved LWP (Figure 3) is approximately 0.25, 0.80, and 1.80 g/m^2 for LWP values of 20, 40, and 50 g/m^2, respectively, which translates into

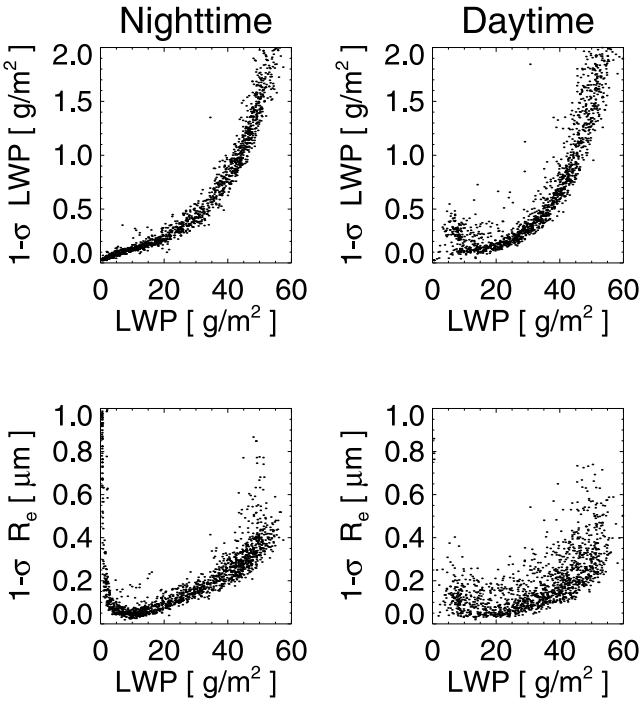

Figure 3. The 1-σ uncertainties in the MIXCRA-retrieved (top) LWP and (bottom) effective radius as a function of LWP, where the results are separated into (left) nighttime (solar elevation lower than 8% above the horizon) and (right) daytime cases. There are 1420 and 1318 cases in the two categories, respectively. The cases were selected such that the uncertainty in r_e was less than 1 μm, $r_e < 15$ μm, and $F_c > 0.95$.

relative errors of 1.3%, 2.0%, and 3.6%. For LWP > 60 g/m^2, the MIXCRA retrieval of LWP is based almost entirely on the microwave observations since the infrared signal has saturated. This results in the 1-σ uncertainty in LWP being on the order of 15 g/m^2 (Figure 1; note that the *y axis* is truncated lower than this value). (The MWR-retrieved LWP is often quoted to have an uncertainty of 25–30 g/m^2 [e.g., *Marchand et al.*, 2003; *Westwater et al.*, 2001]; this uncertainty includes both the random uncertainty of about 15 g/m^2 together with the bias uncertainty of equal or larger value.) The uncertainty in the MIXCRA-retrieved LWP translates into a relative 1-σ uncertainty of 21%, 15%, and 8% for LWP values of 70, 100, and 200 g/m^2, respectively. The large sensitivity of the infrared signal to LWP relative to the microwave signal, given the radiometric uncertainties of the AERI and MWR, essentially results in the algorithm utilizing the infrared observations almost solely when the cloud is semitransparent in the infrared (i.e., has LWP < 60 g/m^2). Therefore small biases in the microwave brightness temperature observations (such as those reported by *Turner et al.* [2007a]) have little influence on the LWP retrievals when the cloud is semitransparent in the infrared, which leads to significantly better retrievals of LWP.

4.2. Diurnal Sensitivity of r_e

[28] MIXCRA retrieves valid values of r_e and τ when the cloud is semitransparent in the infrared, where valid values are determined by looking at the ratio of the 1-σ uncertainty in r_e to the uncertainty in its a priori value. Figure 4 shows the distribution of r_e for both daytime and nighttime cases both as a function of LWP and τ. There is a significant diurnal signal in the dependence of the retrieved r_e value on τ and LWP. During the daytime, the dependence of r_e on the LWP or optical depth is small. For example, the mean value of r_e is approximately 6.4 μm for LWP from 0 to 50 g/m^2 during the daytime, but during the nighttime the mean r_e value increases from 6.3 μm for LWP < 25 g/m^2 to over 8 μm for LWP between 45 and 55 g/m^2 (Table 2).

[29] The information for the retrieval of r_e comes from the shape of the infrared emissivity spectrum in the 8–13 μm band and the amount of sunlight scattered into the AERI's detector in the 3–4 μm band during the daytime. For LWP < 30 g/m^2, the r_e is accurately retrieved. However, as the LWP increases above 30 g/m^2, the emissivity at 13 μm approaches unity because of the strong absorption of liquid water at that frequency. As the LWP continues to increase, an increasingly larger portion of the emissivity spectrum approaches unity, and thus the algorithm produces a high bias in r_e (due to the flatter emissivity spectrum) while maintaining a constant optical depth of approximately 6 [*Turner and Holz*, 2005]. During nighttime conditions, the amount of scattered photons in the 3–4 μm band is negligible, and thus this band offers no additional constraint to the 8–13 μm observations. This has been verified by performing the nighttime retrievals using only the 8–13 μm band, and the results using this single band are the virtually identical as when the retrieval used both bands. However,

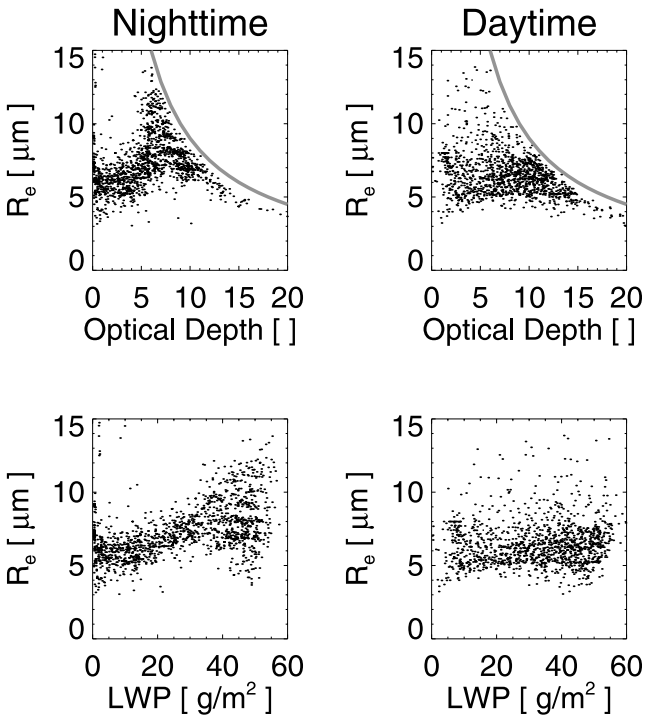

Figure 4. Distribution of r_e as a function of (top) optical depth and (bottom) LWP, separated into (left) nighttime and (right) daytime categories. The data points were the same as those shown in Figure 3. The thick gray line in Figure 4 (top) corresponds to LWP = 60 g/m^2.

Table 2. Statistics on the Retrieved Effective Radius as a Function of LWP for Nighttime and Daytime Conditions

	Nighttime			Daytime		
LWP Range, g/m^2	Mean r_e, μm	Stdev r_e, μm	Npts	Mean r_e, μm	Stdev r_e, μm	Npts
5–15	6.0	1.2	255	6.4	1.4	214
15–25	6.6	0.9	173	6.3	1.5	178
25–35	7.6	1.0	185	6.4	1.5	257
35–45	8.2	1.6	291	6.6	1.6	332
45–55	8.3	2.1	303	6.6	1.5	301

during daytime conditions there is a significant contribution to the detected signal at 3–4 μm by scattered solar photons, where the amount of scattered solar energy incident on the AERI's detector is a function of the particle size. Furthermore, if the 3–4 μm band observations are not used during the daytime, the distribution of r_e retrieved from MIXCRA using only the 8–13 μm observations is similar to the nighttime distribution (i.e., r_e generally increases as LWP increases toward 60 g/m^2) [*Turner and Holz*, 2005]. Therefore the addition of the 3–4 μm band provides an additional constraint on the effective radius during the daytime. This phenomenon explains the difference in the r_e distributions as a function of LWP in Figure 4.

4.3. Comparison of r_e to Aircraft Observations

[30] The AMF deployment at Pt. Reyes was augmented during July by a separate field experiment funded by the DOE called the Marine Stratus Experiment (MASE). MASE provided a wealth of additional aerosol and cloud in situ observations aboard the DOE G–1 Research Aircraft as well as additional in situ aerosol observations on the surface. In particular, the Cloud and Precipitation Spectrometer (CAPS [*Baumgardner et al.*, 2002]) was flown on the G-1, and droplet effective radii were derived from the 10-s averages of the Cloud and Aerosol Spectrometer (CAS) portion of the CAPS. All flight patterns were constant altitude legs; no spirals were flown by the G-1 during this experiment.

[31] To evaluate the MIXCRA-retrieved r_e values, the in situ data were averaged to provide a single value for each flight leg when the G-1 was within 25 km of the AMF site, the droplet number concentration was larger than 25 cm^{-3}, and the aircraft observation was within 4 min of the AERI observation. This resulted in 15 different comparisons from 7 different days. The differences between the two methods have considerable scatter with the difference between the 75th and 25th percentile values being 1.90 μm (not shown); however, the median of the MIXCRA-retrieved minus in situ observed effective radius was 0.11 μm. Some of this variability is due to the horizontal variability in the cloud field that the aircraft transversed; the mean value of the variability in the 15 aircraft observations used in these comparisons is 0.84 ± 0.53 μm. Some of the variability between the aircraft and the MIXCRA-retrieved values is due to the fact that the MIXCRA retrieval is a column-weighted value while the aircraft is sampling only a localized altitude region of the cloud at any given time. These in situ observations, which were all collected during daylight hours, are in good agreement with the MIXCRA retrievals that utilize the 3–4 μm observations during the retrieval. If the 3–4 μm observations were not used, then the MIXCRA retrievals of r_e would be biased high for samples with LWP approaching 60 g/m^2.

4.4. Radiative Closure Validation

[32] The accuracy of the MIXCRA retrievals was evaluated using radiative flux closure studies. Here the retrieved cloud properties are used in a radiative transfer model to compute the surface longwave and shortwave downwelling broadband radiative flux and the top-of-the-atmosphere (TOA) shortwave albedo. The computed fluxes are then compared against observations, and errors in the input cloud properties are assessed through the biases and scatter in the flux residuals.

[33] The observed shortwave and longwave fluxes at the surface and the TOA shortwave albedo are considered "truth" for this exercise, although sampling biases, variability in the instrument's field of view, and calibration uncertainties may affect them. The observed total shortwave flux at the surface was derived by combining the direct beam irradiance measured by a narrow incidence pyrheliometer, weighted by the cosine of the solar zenith angle, with the diffuse flux observed by a shaded pyranometer. The observed surface longwave flux was the average of the observations from two shaded pyrgeometers. All of these radiometers were located at the AMF site, and the data, which were collected at 1-min resolution, are averaged to the 3-min averaging period of the AERI. The TOA shortwave albedo was derived from GOES narrowband radiance observations, where the conversion factors were derived from CERES observations [*Minnis et al.*, 1995]. Since Pt. Reyes is a coastal site, the closest pixel to the AMF site was used in this analysis. However, because of the difficulty in obtaining precise geolocation of the GOES data, the uncertainty in the GOES observations was estimated by computing the standard deviation of the albedo over the 3 × 3 pixel scene centered upon the site. Only the closest MIXCRA sample in time are compared to each GOES observation.

[34] To provide context for the MIXCRA results, the same radiative closure exercise was also conducted using LWP data from an MWR-only retrieval algorithm (MWRRET) [*Turner et al.*, 2007a]. The MWRRET algorithm utilizes an advanced statistical retrieval that incorporates meteorological observations at the surface to help constrain the retrieval of LWP (and precipitable water vapor) from the MWR brightness temperature observations. Additionally, MWRRET also automatically determines if there is a bias in the brightness temperature observations at 31.4 GHz (the liquid water sensitive channel) during clear sky scenes and removes the bias. The advanced statistical retrieval together with the "bias offset" approach result in significantly improved retrieval of LWP from the MWR (relative to the original ARM retrieval product [*Liljegren and Lesht*, 1996]), especially for cases where the LWP is less than 100 g/m^2 [*Turner et al.*, 2007a]. The MWRRET data, which is at the nominal resolution of the MWR (i.e., 20 s), is averaged to the sky-averaging interval of the AERI (3-min).

[35] The broadband calculations were performed with the Rapid Radiative Transfer Model (RRTM) [*Mlawer et al.*, 1997; *Barker et al.*, 2003]. The RRTM is a correlated-k

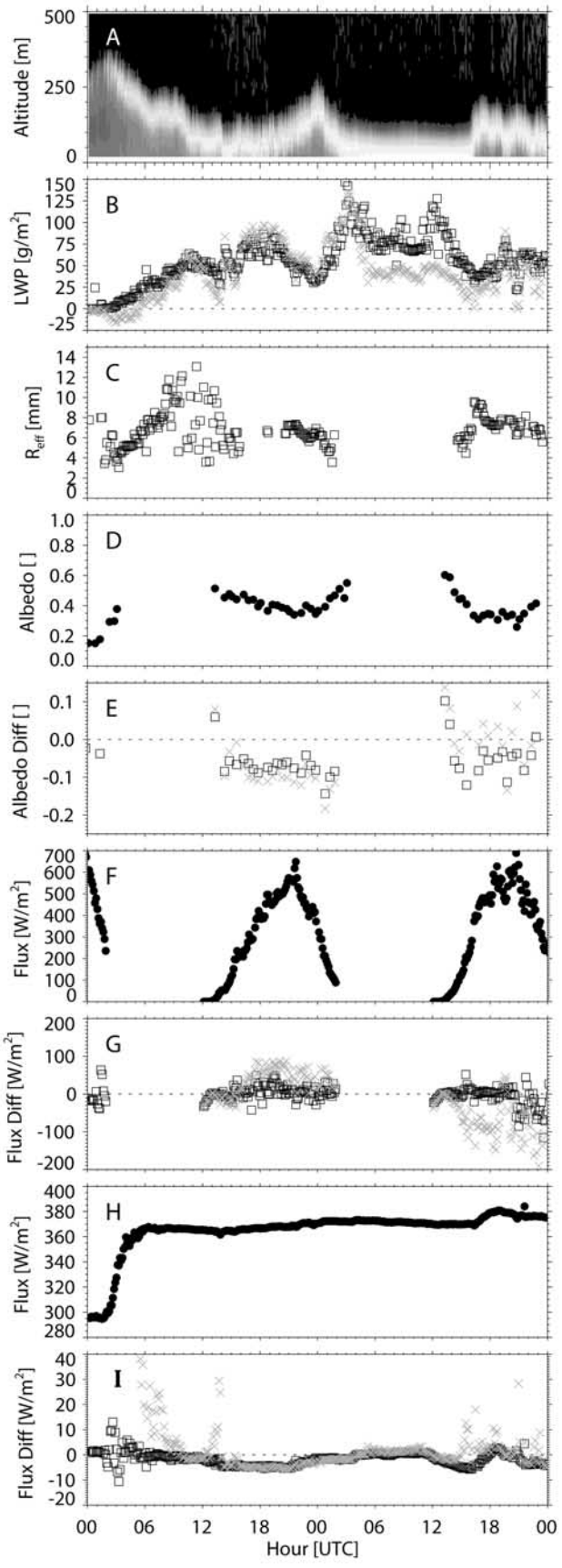

model that was developed using the gaseous optical depths computed from the LBLRTM. Scattering in RRTM is handled by DISORT using 4 streams. The clear sky shortwave spectral surface albedo was determined from MODIS observations. These MODIS spectra were interpolated temporally to the MIXCRA observation time and their broadband shortwave albedo was scaled to match that determined at the AMF site from uplooking and downlooking pyranometers. Because clouds were overhead for almost this entire time period, the aerosol optical depth could not be routinely measured, and thus no aerosols were included in the radiative flux calculations.

[36] The retrieved LWP from both the MIXCRA and MWRRET data sets were distributed uniformly throughout the cloud layer (i.e., profiles of liquid water content constant with altitude), and the cloud layer was assumed to be 300 m thick with the base specified by the ceilometer. This cloud thickness was the approximate median thickness for this two-month period suggested by an analysis of colocated 95 GHz cloud radar Doppler velocities; unfortunately, reflectivity data from this radar could not be calibrated (M. Miller, personal communication, 2006). The MWRRET calculations used the r_e from the coincident MIXCRA retrieval; when the LWP was too large for MIXCRA to retrieve r_e for a particular sample, the median r_e value for the day was used in both the MIXCRA and MWRRET closure calculations. For these calculations, r_e was also assumed to be constant with altitude through the cloud. If the retrieved LWP was less than zero, then the radiative fluxes were not computed for that sample; this condition only affected the MWRRET flux calculations.

4.4.1. Case Study: 5–6 July 2005

[37] As indicated above, low overcast clouds existed above the AMF site for almost the entire July to August period. An example from a two-day period is provided in Figure 5. At the start of this period (from 0000 to 0200 UTC on 5 July), the sky was clear as indicated by the ceilometer by the lack of strong (white) backscatter from the lidar (Figure 5a); however, there was a significant aerosol layer up to approximately 300 m (light gray). However, low-level clouds advected into the region after 0200 UTC and the

Figure 5. Data from 5 to 6 July 2005 at the Pt Reyes site. (a) Backscatter observed by the Vaisala ceilometer. (b) LWP retrieved by the MIXCRA (black squares) and MWRRET (gray crosses) algorithms. (c) Effective radius from MIXCRA; gaps in the data are indicative of periods where the cloud was opaque in the infrared and thus r_e could not be retrieved. (d) TOA shortwave albedo observed by the GOES-10 (nearest pixel value). (e) Observed minus calculated TOA albedo residuals. (f) Observed total shortwave flux at the surface. (g) Observed minus calculated total shortwave flux residuals at the surface. (h) Observed longwave flux at the surface. (i) Observed minus calculated longwave flux at the surface. For Figures 5e, 5g, and 5i, the computed fluxes used both the MIXCRA-retrieved (black squares) and MWRRET-retrieved (gray crosses) LWP values. In both cases the effective radius utilized was the instantaneous MIXCRA retrieval but, if this value was not available, then the median r_e value from MIXCRA for the entire day was utilized.

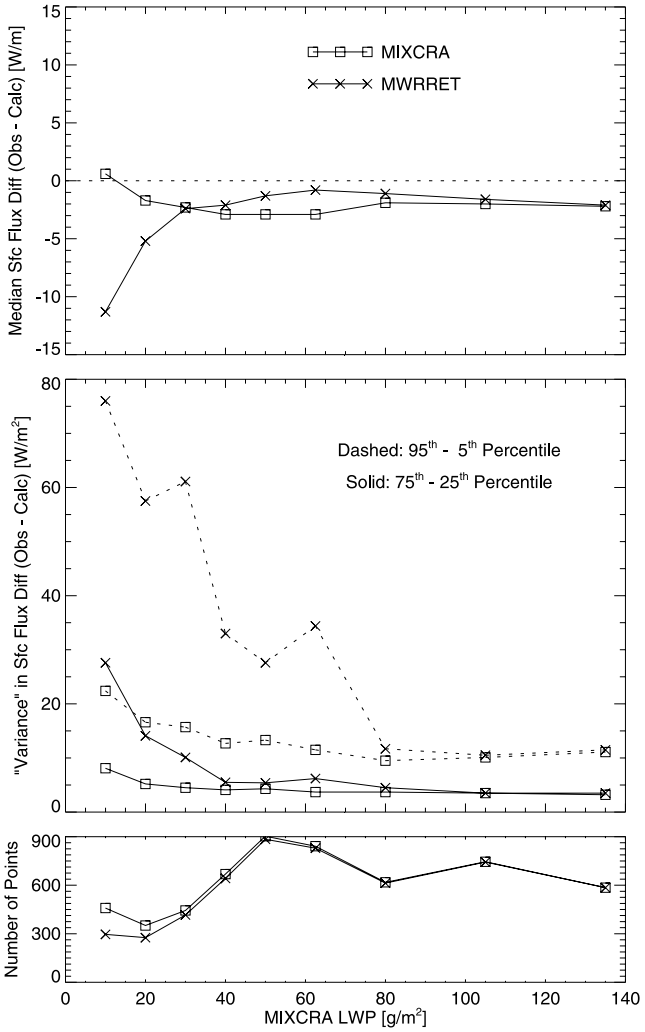

Figure 6. Downwelling surface longwave flux residuals (observed minus calculated), where MIXCRA-retrieved (open squares) and MWRRET-retrieved (crosses) LWP data were used in the flux calculations. (top) Median values for each LWP bin (bin ranges are defined in the text). (middle) Two estimates of the variance (or spread) in the residuals: the solid lines show the 75th minus 25th percentile spread, while the dotted lines show the 95th minus 5th percentile spread. (bottom) Number of points in each bin for each method. The LWP bins are 5–15 g/m^2, 15–25 g/m^2, 25–35 g/m^2, 35–45 g/m^2, 45–55 g/m^2, 55–70 g/m^2, 70–90 g/m^2, 90–120 g/m^2, and 120–150 g/m^2.

LWP increased from 0 g/m^2 at 0000 UTC on the 5 July to over 50 g/m^2 at 1200 UTC on 5 July (Figure 5b). During this period, the MIXRA-retrieved LWP (black squares, Figure 5b) was often significantly different than the MWRRET-retrieved value (gray crosses, Figure 5b). From 0000 to 1200 UTC on 5 July, the MIXCRA-retrieved r_e value changed dramatically from approximately 4 μm to over 10 μm (Figure 5c). During this period, the LWP was less than 50 g/m^2 and thus the uncertainty in the retrieved r_e is less than 0.5 μm (Figure 3). Furthermore, the increase in the r_e over this period coincides with a significant decrease in the observed cloud condensation nuclei (CCN) counts measured at the surface as part of MASE (not shown). The correlation between the change in r_e and CCN counts suggests that rapid change in r_e is likely a real response to changing aerosol conditions; however, a full investigation of this particular feature is beyond the scope of this paper and will be the subject of future work.

[38] Figure 5 shows the observed TOA shortwave albedo, surface shortwave flux, and surface longwave flux (Figures 5d, 5f, and 5h) and the corresponding observed minus calculated residuals (Figures 5e, 5g, and 5i). For this 2-day example, the TOA albedo (Figure 5e) calculated from the MIXCRA cloud properties shows an apparent bias of approximately −0.06 for both days (note that local noon is approximately 2000 UTC). The MWRRET TOA albedo also shows this bias on 5 July, but is in better mean agreement with the GOES-derived albedo on 6 July. However, the MWRRET data have more scatter in the derived albedo relative to the GOES observations than the MIXCRA computations.

[39] The shortwave surface flux residuals (Figure 5g) also demonstrate that the MWRRET-computed fluxes appear to have more scatter relative to the observations than the flux computations that used MIXCRA data. The flux residuals from MIXCRA and MWRRET each have an approximate mean value of 0 W/m^2, but MWRRET attains its near-zero bias by significant cancellation of error (positive residuals on 5 July and negative residuals on 6 July).

[40] The longwave surface flux residuals (Figure 5i) also seem to demonstrate that the MWRRET residuals have more scatter than the MIXCRA residuals. This is most apparent during the time periods where the LWP $\ll$ 50 g/m^2, such as from 0000 to 0800 UTC on 5 July. Note that between 0000 and 0500 UTC the MWRRET-retrieved LWP was less than zero, and thus the flux calculations were not performed for this data set. When the LWP is significantly larger than 50 g/m^2, the cloud is virtually opaque from an infrared radiance point of view (Figure 1) and differences in the LWP above this threshold are irrelevant as the radiative flux is now only sensitive to the cloud temperature.

[41] This case study provides an example of how well the computed radiative fluxes from the MIXCRA- and MWRRET-derived cloud properties agree with the observed fluxes on a point-to-point basis. To better characterize the differences in flux residuals, data from the entire two-month period (July–August 2005) were grouped as a function of LWP to investigate the median bias and "variance" in the residuals for surface longwave flux (Figure 6), surface shortwave flux (Figure 8), and TOA shortwave albedo (Figure 10). Two measures of "variance" are provided so that a Gaussian distribution of residuals did not need to be assumed. These variance, or spread, values were computed as the 3rd minus 1st quartile (i.e., 75th minus 25th percentile) values, and as the 95th minus 5th percentile values. The LWP bins for the following analysis are 5–15 g/m^2, 15–25 g/m^2, 25–35 g/m^2, 35–45 g/m^2, 45–55 g/m^2, 55–70 g/m^2, 70–90 g/m^2, 90–120 g/m^2, and 120–150 g/m^2. For clouds with LWP above 150 g/m^2, the MIXCRA and MWRRET results are virtually identical, since the infrared component of MIXCRA is no longer offering any information to the retrieval algorithm and, thus, the retrieval is essentially reduced to a physical retrieval using only MWR data.

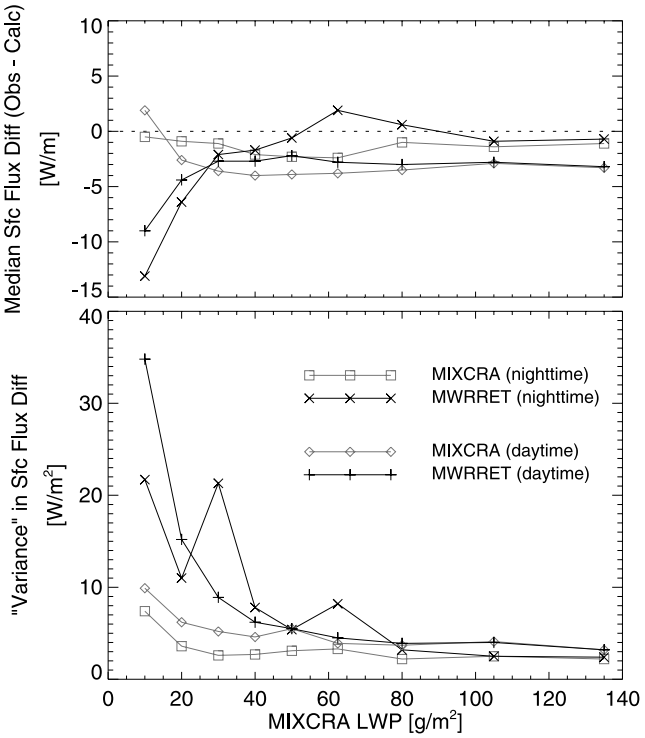

Figure 7. Downwelling surface longwave flux residuals from Figure 6, separated into daytime and nighttime conditions, for both the MIXCRA- and MWRRET-based calculations. The ''variance'' shown in the bottom plot is the interquartile spread. The nighttime statistics for MIXCRA are slightly better than the daytime statistics (smaller median bias and less variability); however, the difference between the daytime and nighttime results are small.

4.4.2. Surface Longwave Flux Closure

[42] We begin the evaluation of the MIXCRA-retrieved cloud properties by looking at the ability of the algorithm to close in downwelling longwave flux at the surface. We recognize that this is a somewhat circular exercise, as infrared spectral radiance information was used in the MIXCRA retrievals and thus the calculations that use the MIXCRA-derived cloud properties should close in longwave flux (assuming that the cloud scene is uniform and the retrieval is accurate). However, this exercise provides a way to evaluate the diurnal behavior of the MIXCRA and MWRRET cloud properties, which cannot be evaluated with a shortwave flux closure exercise.

[43] The statistical results from the surface longwave flux closure exercise are shown in Figure 6. The median bias in the MIXCRA-derived flux is less than 3 W/m^2 for the entire range of LWP. The uncertainty in the observed flux by the pyrgeometers is approximately 4 W/m^2 [*Stoffel*, 2005, Table 4], and thus the bias is within the calibration uncertainty of the pyrgeometers. However, for LWP < 25 g/m^2, the MWRRET-derived flux is considerably larger than the MIXCRA-derived value. Both variance estimates (Figure 6, middle) for the MIXCRA-based residuals are much smaller than the MWRRET-based residuals for LWP < 40 g/m^2, and the 95th minus 5th percentile spread for MIXCRA results is significantly smaller for LWP up to 70 g/m^2. The relatively small variance in the MIXCRA-derived residuals (relative to the MWRRET-derived results) demonstrates the improved skill in the MIXCRA-derived cloud properties that were used in the flux computations. Additionally, the number of points in each LWP bin also shows that there are significantly more values from the MIXCRA retrievals for LWP < 40 g/m^2; the difference in the number of points indicates the relative number of times that the MWRRET retrievals produced LWP < 0 g/m^2. Note that the median bias and variability results from MIXCRA and MWRRET converge to each other when the LWP > 100 g/m^2.

[44] Table 2 and Figure 4 illustrate that there is a difference in the distribution of r_e between nighttime and daytime retrievals; we examine whether these differences impact the surface longwave flux residuals. The median bias and 75th minus 25th percentile spread of the daytime and nighttime surface longwave flux residuals for both the MIXCRA- and MWRRET-based calculations are provided in Figure 7. Qualitatively, the daytime and nighttime results from both MIXCRA and MWRRET mirror the general behavior shown in Figure 6 for both the median residual and spread. However, for the MIXCRA-based results, the median bias and spread is slightly smaller at night than during the day (about 1–2 W/m^2 and 2 W/m^2, respectively). The reduction of the spread may be related to the diurnal variability in the cloud structure, as solar heating leads to a more varied, decoupled marine boundary layer.

[45] As indicated in section 4.2, the nighttime retrievals of r_e from MIXCRA become biased toward larger values as LWP increases toward 60 g/m^2 because of the ''flattening'' of the cloud emissivity spectrum [*Turner and Holz*, 2005]. However, at night, this r_e bias is not important from an infrared radiative flux point of view since the retrieved clouds properties satisfied the infrared spectral radiance observations between 8 and 13 μm, and it is in this spectral range that the flux is most sensitive to the cloud properties. Therefore, even though the nighttime r_e values are biased relative to the daytime r_e values as a function of LWP, both daytime and nighttime MIXCRA-derived cloud properties close in surface longwave flux (within the uncertainty of the observations) for LWP < 60 g/m^2.

4.4.3. Surface Shortwave Flux Closure

[46] The downwelling surface shortwave flux closure statistics are shown in Figure 8. The MIXCRA retrieval algorithm does utilize some information in the tail of the shortwave band (in the 3–4 μm spectral region) during the daytime, which provides more accurate r_e retrievals as the LWP approaches 60 g/m^2 (section 4.2). Therefore it also introduces a small amount of potential circularity in the shortwave flux closure results. However, since there is relatively little solar flux in the 3–4 μm band, as compared to the visible and near-infrared spectral region from 0.3 to 3 μm, the use of shortwave flux closure is more independent than the longwave flux closure exercise discussed in section 4.4.2.

[47] The median bias in the surface shortwave flux closure results (Figure 8, top) shows that the MIXCRA-derived flux is larger than the observed flux for LWP < 30 g/m^2, where the median bias for the MWRRET retrievals is much closer to 0 W/m^2. The calculations with both sets of cloud properties yield good agreement with the observed fluxes for 30 g/m^2 < LWP < 70 g/m^2, but both sets of

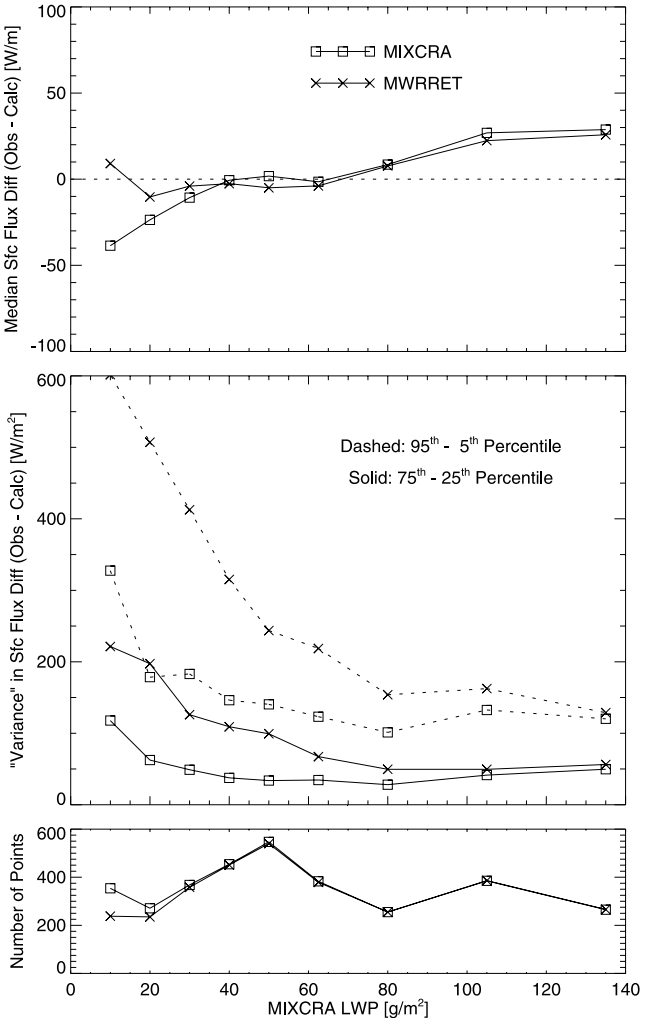

Figure 8. Same as in Figure 6 but showing downwelling total shortwave flux residuals at the surface.

computed fluxes begin to underestimate the observed flux for LWP > 70 g/m^2. Like the surface longwave flux results, the MIXCRA-retrieved cloud properties yield significantly less scatter in the flux residuals than the MWRRET-based calculations (Figure 8, middle).

[48] The variance results (Figure 8, middle) clearly show that the MIXCRA retrievals have more skill than MWRRET-based retrievals for LWP < 70 g/m^2, but also suggest that the same is true for LWP as large at 120 g/m^2. This improved skill for the larger LWP cases might seem unfeasible, since the infrared component of the MIXCRA retrieval becomes saturated for LWP > 60 g/m^2 and, thus, the MIXCRA retrieval reduces to a microwave-only method for large LWPs. The answer lies in the optimal estimation methodology and how it weights the measurement uncertainties and forward model sensitivities. The methodology works to find a state vector **X** such that all of the observations **Y** (equation (2)) are matched within their uncertainties. Suppose that the true LWP is 80 g/m^2. At this point, the infrared observations would be saturated and thus the algorithm "knows" that the LWP must be above the infrared saturation point of approximately 60 g/m^2. However, if the microwave observations alone suggest that the LWP is below this saturation point, then the optimal estimation will "insist" that the retrieved LWP be larger than this saturation point because the uncertainty in the infrared observations is considerably smaller than the microwave observations (from the LWP point of view). Thus for LWP cases that are above the infrared saturation point, the MIXCRA algorithm prevents the retrieved LWP from being smaller than the saturation point, and thus narrows the low end of the distribution of retrieved LWP. This, however, has little to no effect on the median shortwave surface flux residuals for these larger LWP cases.

[49] We now examine the reason for the differences in median biases between the two residuals in the surface shortwave flux for LWP < 25 g/m^2 (Figure 8, top). First, it should be noted that the MIXCRA-based results have significantly more points in the smallest two LWP bins than the MWRRET-based results; this is because the flux was not computed for cases where the MWRRET-retrieved LWP was less than zero. Let us assume for the moment that the MWRRET-retrieved LWP is correct in a mean sense (i.e., has a true zero bias) but has large scatter so that some points have LWP less than zero. If we remove the retrievals that have LWP less than zero from the distribution, then the mean value computed from the remaining data set will be higher than the true mean value. Thus the removal of these points with LWP less than zero will result in a high bias in the mean computed flux. Therefore, in a statistical sense, the low end of the distribution of LWP from the MWRRET algorithm has been removed (since a shortwave flux calculation is impossible if the LWP is negative), which creates a bias in the MWRRET-based shortwave flux residuals toward cases with larger LWP. Thus the apparent good agreement in shortwave surface flux using the MWRRET-retrieved results is probably biased high and thus fortuitously results in better agreement with observations.

[50] Secondly, for small LWP cases, the visible cloud optical depth is also relatively small, and thus ignoring the contribution of aerosols to the shortwave flux will result in bias error in the computed flux. The ARM program measured aerosol scattering properties at the surface at Pt. Reyes using a variety of in situ instruments similar to those at the ARM Southern Great Plains site [*Sheridan et al.*, 2001]. From these observations, the intensive aerosol properties, such as single scattering albedo, asymmetry parameter, and Ångström exponent, are derived. However, because of the pervasive low-altitude cloud cover (which provides a large number of overcast cloud scenes to use in this study), the aerosol optical depth, which is usually determined from direct-beam solar irradiance observations, could not be determine routinely. Thus we do not have a good time series of aerosol optical depth to include in the shortwave flux calculations.

[51] To estimate the possible impact that aerosols would have on the shortwave surface flux closure exercise, a set of RRTM calculations was performed using mean aerosol properties derived from the surface in situ observations and two assumed optical depths. The cloud base height, cloud thickness, and droplet effective radius were fixed to 100 m, 300 m, and 6.2 μm, respectively, and the LWP was ramped from 0 to 150 g/m^2. The aerosol layer was assumed to be between the surface and the cloud; no aerosols were included above the cloud. Since aerosol optical depths are

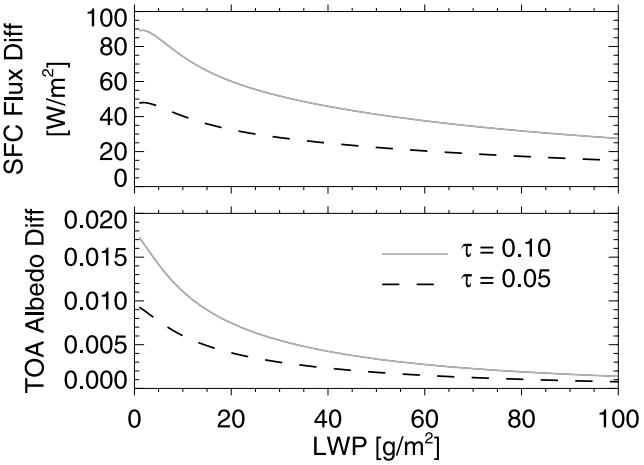

Figure 9. (top) Change in the computed total shortwave downwelling surface flux and (bottom) TOA albedo from clear sky conditions as a function of cloud LWP for aerosol layers with two different assumed visible optical depths (0.05 and 0.10 at 500 nm). The differences are expressed as (clear sky value) minus (aerosol-laden value). The aerosol was assumed to lie between the surface and the cloud layer. The calculations used a single scattering albedo of 0.968, an asymmetry parameter of 0.636, and an Ångström exponent of 1.46 for the aerosol; these are the mean properties of the aerosol observed at the AMF site by in situ sensors at the surface from July to August 2005. The cloud droplet r_e value used in the calculations was 6.2 μm.

typically small in marine environments, the calculations used aerosol visible optical depths of 0.05 and 0.10. Adding aerosols would decrease the computed surface shortwave flux relative to the aerosol-free calculations (Figure 9), where the magnitude depends on the aerosol optical depth and the LWP. Therefore adding an aerosol layer with a small (but reasonable) optical depth into the flux calculations would improve the flux residuals using MIXCRA-derived LWP for LWP less than 30 g/m^2 (but it would also worsen the MWRRET results). However, this same amount of aerosol would then result in worse agreement for the MIXCRA results for larger LWP but the results would appear to approach an asymptote around 30 W/m^2. (The uncertainty in the diffuse shortwave flux observation is 20 W/m^2 or 6% [*Stoffel*, 2005].) However, without accurate aerosol optical depth measurements, the actual impact on the downwelling shortwave flux bias cannot be determined exactly.

4.4.4. TOA Shortwave Albedo Closure

[52] The TOA shortwave albedo statistics are shown in Figure 10. Like the surface flux results shown in Figures 6 and 8, the MIXCRA-based calculations show significantly less spread for the cases with LWP < 90 g/m^2, which again suggests superior skill in the MIXCRA retrieval of LWP relative to the MWRRET. However, the median bias for both sets of retrievals is significantly negative, with the computed albedo being approximately 0.07 higher than what was observed by the GOES-10 satellite.

[53] As indicated earlier, the GOES data used in this analysis is a single pixel (4 km resolution) value because the AMF is at a coastal site. However, because of the uncertainty of the geolocation of the pixel, the uncertainty in the GOES albedo is estimated by computing the standard deviation of the albedo in the 3 × 3 array of pixels centered upon the AMF site. (It should be noted that the single-pixel albedo was on average 0.01 larger than the mean value computed over the 3 × 3 array of pixels for LWP < 150 g/m^2.) The shaded region in Figure 10 (top) indicates the 1-sigma uncertainty in the GOES observations as estimated from the variability in the 3 × 3 pixel scene; this uncertainty estimate does not include the uncertainty that is part of the conversion of narrowband radiances to flux [*Minnis et al.*, 1995]. The mean bias of the MIXCRA-based calculations is just outside this envelope for LWP < 60 g/m^2.

[54] To reduce the computed albedo by the amount needed to match the observations, the LWP would have to be significantly reduced; however, that would greatly worsen the results for the shortwave and longwave surface fluxes. Sensitivity studies on the surface albedo and the vertical distribution of effective radius cannot explain this difference. Adjusting the surface albedo within reasonable

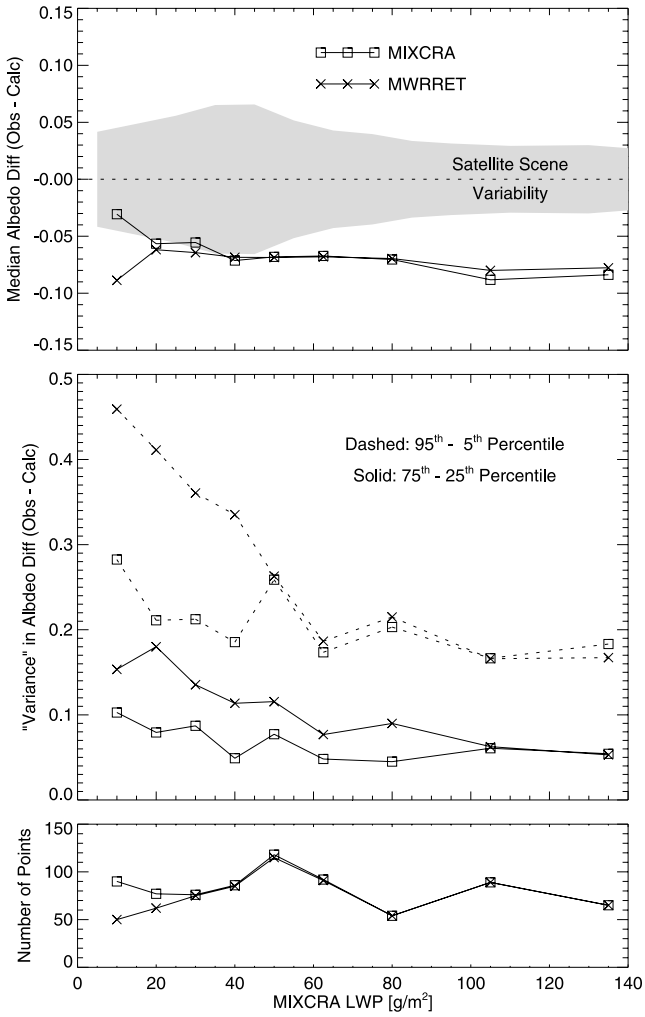

Figure 10. Same as in Figure 6 but showing shortwave TOA albedo residuals. The gray region in Figure 10 (top) denotes the 1-sigma standard deviation of the GOES observations in the 3 × 3 pixel region around the AMF site. See text for details.

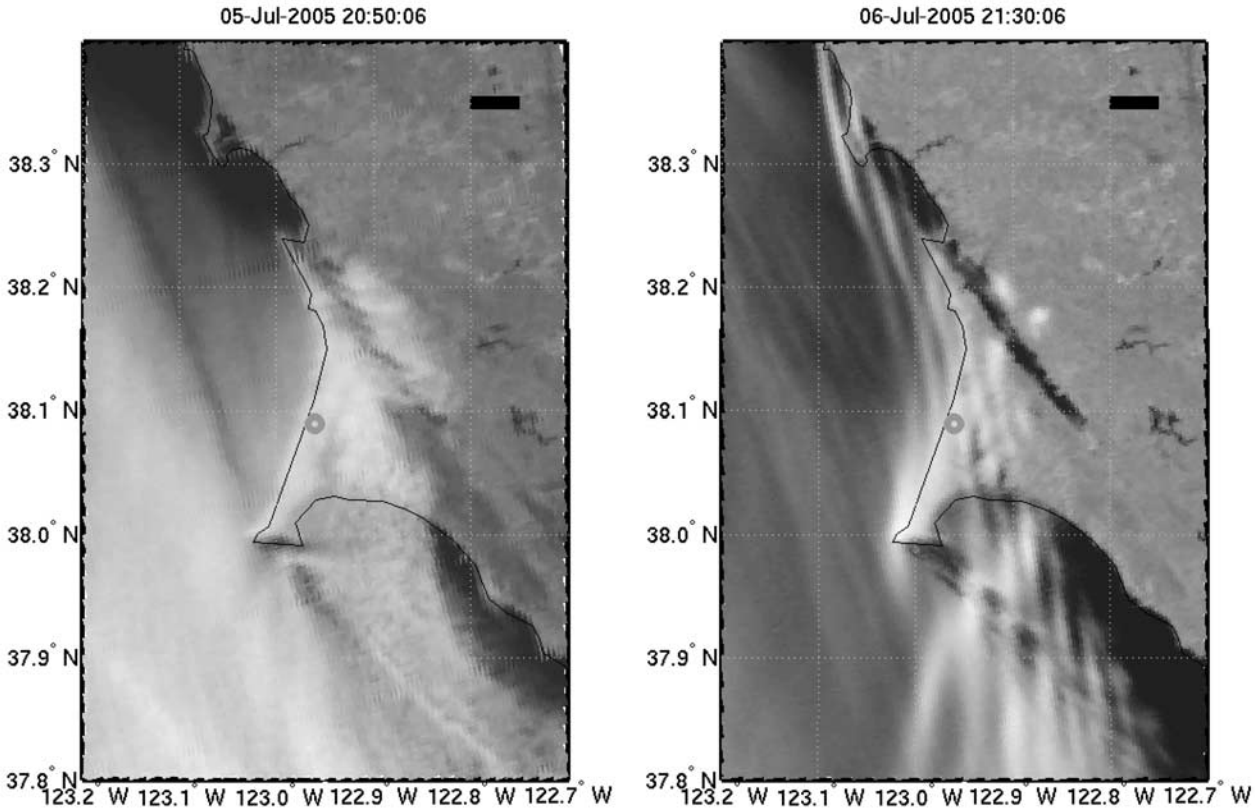

Figure 11. MODIS 250 m resolution reflectance data at 870 nm over the Pt. Reyes region for (left) 5 July 2005 at 2050 UTC and (right) 6 July 2005 at 2130 UTC. The location of the AMF is denoted with the thick, dark circle in the center of each image. For scale, the horizontal black bar in the upper right corner of each image is 10 km long. There is a significant change in the 870 nm reflectance (and the 670 nm reflectance, not shown) from the ocean region just off the coast from Pt. Reyes relative to the regions over land.

bounds had a negligible impact on the TOA results. The results in Figure 10 (as with Figures 6 and 8) assumed that the effective radius was constant with height in the cloud; however, distributing the cloud liquid water adiabatically and assuming a constant number cloud droplet number density in order to get a height-dependent r_e profile for the cloud did not change the TOA results significantly (or the surface results either). Adding a small amount of aerosol below the cloud does impact the TOA albedo slightly (Figure 9, bottom), reducing the calculated albedo by a small amount depending on aerosol optical depth and cloud LWP. This could potentially bring the MIXCRA-computed albedo into agreement within the uncertainty of the GOES observations for LWP < 60 g/m^2.

[55] As indicated earlier, the AMF location is within 1 km of the coast of California, and inhomogeneities might exist in the cloud field associated with the land/ocean interface or in the clouds as they move further inland. The bias in the TOA albedo residuals (especially in the MIXCRA-based results) was clear even in our case study on 5 to 6 July (Figure 5e). MODIS images showing the 870-nm reflectance at 250 m resolution over the AMF site for the afternoons of these two days are shown in Figure 11. The MODIS data show a clear difference in the cloud reflectance between clouds over land and over the ocean, where the clouds over the ocean are significantly less reflective, and thus have presumably lower LWP. The GOES footprint may contain contributions from both the ocean and land, and thus its derived albedo may be smaller than the albedo of the clouds that are only over the AMF site. Therefore we feel that the bias in the TOA albedo measurements (Figure 10, top) may be partially explained by the inhomogeneity of the clouds in the GOES field of view, as well as an unknown contribution from the atmospheric aerosol, and is not due to inaccuracies (biases) in the MIXCRA-retrieved cloud properties.

5. Conclusions

[56] We have extended the mixed-phase cloud retrieval algorithm (MIXCRA) to retrieve liquid water cloud properties that satisfy both infrared (8–13 μm and 3–4 μm) and microwave (23.8 and 31.4 GHz) radiance observations from ground-based sensors. The algorithm retrieves LWP from less than 5 to over 1000 g/m^2, and achieves a particularly small random error (less than 4%) for LWP less than 50 g/m^2 (owing to the strong sensitivity of infrared radiance to LWP below this threshold). Above 60 g/m^2, the infrared radiance is saturated with respect to its sensitivity to LWP changes; however, the infrared observations continue to

provide information resulting in superior LWP values relative to a microwave-only retrieval for LWP up to 120 g/m^2.

[57] MIXCRA also retrieves the r_e of the liquid water clouds when the cloud is semitransparent in the infrared (i.e., when the LWP is less than 60 g/m^2). There are differences in the daytime versus nighttime distributions of r_e, where the solar radiance signal in the 3–4 μm channels during the daytime improves the r_e retrievals by reducing the small bias in the retrieved r_e as the LWP approaches the infrared saturation point of 60 g/m^2. The median difference of the MIXCRA-retrieved r_e values with aircraft in situ observations is 0.11 μm (with an interquartile spread of 1.90 μm) for the 15 cases, all of which occurred during the daytime. While nighttime observations of warm liquid water cloud properties have not been made over the ARM sites to date, these observations are required to fully characterize the accuracy of the nighttime retrievals of r_e.

[58] To evaluate the accuracy of the MIXCRA-retrieved LWP, the cloud properties were used in a radiative transfer model to compute the downwelling surface longwave and shortwave fluxes and the TOA shortwave albedo, which were compared against observations. A reference calculation used microwave-only retrievals of LWP from a recently developed retrieval algorithm (MWRRET). The observed minus calculated flux residuals, both at the surface and the TOA, show significantly less scatter with the MIXCRA-derived LWP relative to the MWRRET-derived LWP. This large reduction in scatter, which is significant for LWP $<$ 50 g/m^2 and appreciable for clouds with LWP as large as 120 g/m^2, demonstrates that the MIXCRA algorithm has superior skill in retrieving LWP relative to the microwave-only approach used in MWRRET. This improvement in retrieving LWP for LWP less than 100 g/m^2 is critical, as a large fraction of clouds liquid water clouds observed at all of the ARM sites (tropics, midlatitudes, and arctic) have LWP below this threshold.

[59] This analysis has demonstrated the ability of the MIXCRA algorithm to provide quantitative cloud properties in a stratiform, warm cloud environment with good accuracy for clouds with small LWP. However, there are still some open questions that will be addressed in future work. The MIXCRA retrievals will be applied to data collected at the other ARM sites, such as the Southern Great Plains (SGP) site in Oklahoma. The aerosol field is well characterized at the SGP site by the operational Raman lidar [*Turner et al.*, 2002], and the variability of the cloud inside the GOES field of view is likely more evenly distributed, relative to the coastal Pt. Reyes site, which should reduce the uncertainties in the TOA shortwave flux closure. We will work to coordinate nighttime aircraft in situ observations in order to evaluate the accuracy of the retrieved effective radius. We will also investigate the accuracy of this algorithm in broken cloud fields (e.g., cumulus), where three-dimensional effects and precisely accounting for differences between the AERI and MWR fields of view become more critical.

[60] **Acknowledgments.** The U.S. Department of Energy, Office of Science, Office of Biological and Environmental Research, Environmental Sciences Division funded this project as part of the ARM program under grant DE-FG02-06ER64167. The AERI, MWR, broadband radiometer, ceilometer, and radiosonde data using in this analysis were collected by the ARM program, and the DOE Atmospheric Science Program (ASP) collected the aircraft in situ data that were utilized in this study. We would like to thank Patrick Minnis and Mandana Khaiyer for providing the GOES TOA albedo data, J.-Y. Chiu for providing the MODIS surface albedo spectra, Allison McComisky for the mean aerosol properties, and Robert Holz for creating the MODIS images. Andy Vogelmann and Jennifer Delamere provided comments on an early draft of this manuscript, and their efforts are greatly appreciated. The comments from three anonymous reviewers also improved the clarity of the manuscript and are appreciated.

References

Ackerman, T. P., and G. M. Stokes (2003), The Atmospheric Radiation Measurement Program, *Phys. Today*, *56*, 38–45.

Barker, H. W., et al. (2003), Assessing 1-D atmospheric solar radiative transfer models: Interpretation and handling of unresolved clouds, *J. Clim.*, *16*, 2676–2699.

Baumgardner, D., H. Jonsson, W. Dawson, D. O'Conor, and R. Newton (2002), The Cloud, Aerosol and Precipitation Spectrometer (CAPS): A new instrument for cloud investigations, *Atmos. Res.*, *59–60*, 251–264.

Cess, R. D., et al. (1996), Cloud feedback in atmospheric general circulation models: An update, *J. Geophys. Res.*, *101*, 12,791–12,794.

Clough, S. A., M. W. Shephard, E. J. Mlawer, J. S. Delamere, M. J. Iacono, K. Cady-Pereira, S. Boukabara, and P. D. Brown (2005), Atmospheric radiative transfer modeling: A summary of the AER codes, *J. Quant. Spectrosc. Rad. Transfer*, *91*, 233–244.

Donovan, D. P., and A. C. A. P. van Lammeren (2001), Cloud effective particle size and water content profile retrievals using combined lidar and radar observations: Part 1. Theory and examples, *J. Geophys. Res.*, *106*, 27,425–27,448.

Frisch, A. S., C. W. Fairall, and J. B. Snider (1995), Measurements of stratus cloud and drizzle parameters in ASTEX with a Ka-band Doppler Radar and a microwave radiometer, *J. Atmos. Sci.*, *52*, 2788–2799.

Gaussiat, N., R. J. Hogan, and A. J. Illingsworth (2007), Accurate liquid water path retrieval from low-cost microwave radiometers using additional information from a lidar ceilometer and operational forecast models, *J. Atmos. Oceanic Technol.*, in press.

Gerber, H. (1996), Microphysics of marine stratocumulus clouds with two drizzle modes, *J. Atmos. Sci.*, *53*, 1649–1662.

Han, Y., J. B. Snider, E. R. Westwater, S. H. Melfi, and R. A. Ferrare (1994), Observations of water vapor by ground-based microwave radiometers and Raman lidar, *J. Geophys. Res.*, *99*, 18,695–18,702.

Hewison, T., D. Cimini, L. Martin, C. Gaffard, and J. Nash (2006), Validating clear air absorption models using ground-based microwave radiometers and vice-versa, *Meteorol. Z.*, *15*, 27–36, doi:10.1127/0941-2948/2006/0097.

Illingsworth, A. J., et al. (2007), CLOUDNET–Continuous evaluation of cloud profiles in seven operational models using ground-based observations, *Bull. Am. Meteorol. Soc.*, *88*, 883–898, doi:10.1175/BAMS-88-6-883.

Knuteson, R. O., et al. (2004a), Atmospheric emitted radiance interferometer. Part I: Instrument design, *J. Atmos. Oceanic Technol.*, *21*, 1763–1776.

Knuteson, R. O., et al. (2004b), Atmospheric Emitted Radiance Interferometer. Part II: Instrument performance, *J. Atmos. Oceanic Technol.*, *21*, 1777–1789.

Liebe, H. J., G. A. Hufford, and T. Manabe (1991), A model for the complex permittivity of water at frequencies below 1 THz, *Int. J. Infrared Millimeter Waves*, *12*, 659–675.

Liljegren, J. C. (2000), Automatic self-calibration of ARM microwave radiometers, in *Microwave Radiometry and Remote Sensing of the Earth's Surface and Atmosphere*, edited by P. Pampaloni and S. Paloscia, pp. 433–443, VSP Press, Utrecht, The Netherlands.

Liljegren, J. C., and B. M. Lesht (1996), Measurements of integrated water vapor and cloud liquid water from microwave radiometers at the DOE ARM cloud and radiation testbed in the U.S. Southern Great Plains, in *Proceedings of the International Geoscience and Remote Sensing Symposium (IGARSS)*, pp. 1675–1677, IEEE, Lincoln, Nebr.

Löhnert, U., and S. Crewell (2003), Accuracy of cloud liquid water path from ground-based microwave radiometery: 1. Dependence on cloud model statistics, *Radio Sci.*, *38*(3), 8041, doi:10.1029/2002RS002654.

Marchand, R., T. Ackerman, E. R. Westwater, S. A. Clough, K. Cady-Pereira, and J. C. Liljegren (2003), An assessment of microwave absorption models and retrievals of cloud liquid water using clear-sky data, *J. Geophys. Res.*, *108*(D24), 4773, doi:10.1029/2003JD003843.

Matrosov, S. Y., T. Uttal, and D. A. Hazen (2004), Evaluation of radar reflectivity-based estimates of water content in stratiform marine clouds, *J. Appl. Meteorol.*, *43*, 405–419.

McFarlane, S. A., and K. F. Evans (2004), Clouds and shortwave fluxes at Nauru. Part I: Retrieved cloud properties, *J. Atmos. Sci.*, *61*, 733–744.

Miller, M. A., and A. Slingo (2007), The Atmospheric Radiation Measurement (ARM) Mobile Facility (AMF) and its first international deployment: Measuring radiative flux divergence in West Africa, *Bull. Am. Meteorol. Soc.*, in press.

Min, Q., and L. C. Harrison (1996), Cloud properties derived from surface MFRSR measurements and comparison with GOES results at the ARM SGP site, *Geophys. Res. Lett.*, *23*, 1641–1644.

Minnis, P., et al. (1995), Clouds and the Earth's Radiant Energy System (CERES) algorithm theoretical basis document, *NASA-RP-1376-vol-3*, pp. 135–176, Natl. Aeronaut. Space. Admin., Silver Spring, Md.

Mlawer, E. J., S. J. Taubman, P. D. Brown, M. J. Iacono, and S. A. Clough (1997), Radiative transfer for inhomogeneous atmospheres: RRTM, a validated correlated-k model for the long wave, *J. Geophys. Res.*, *102*, 16,663–16,682.

Sengupta, M., E. E. Clothiaux, T. P. Ackerman, S. Kato, and Q. Min (2003), Importance of accurate liquid water path for estimation of solar radiation in warm boundary layer clouds: An observational study, *J. Clim.*, *16*, 2997–3009.

Sheridan, P. J., D. J. Delene, and J. A. Ogren (2001), Four years of continuous surface aerosol measurements from the DOE/ARM Southern Great Plains CART site, *J. Geophys. Res.*, *106*, 20,735–20,747.

Shupe, M. D., and J. M. Intrieri (2004), Cloud radiative forcing of the Arctic surface: The influence of cloud properties, surface albedo, and solar zenith angle, *J. Clim.*, *17*, 616–628.

Stephens, G. L. (2005), Cloud feedbacks in the climate system: A critical review, *J. Atmos. Sci.*, *18*, 237–273.

Stoffel, T. (2005), Solar infrared radiation station (SIRS) handbook, *ARM Tech. Rep. TR-025*, 29 pp., Atmos. Radiat. Measure. Program, U.S. Dep. of Energy, Washington, D. C. (available at http://www.arm.gov/publications/tech_reports/handbooks/sirs_handbook.pdf).

Stokes, G. M., and S. E. Schwartz (1994), The Atmospheric Radiation Measurement (ARM) Program: Programmatic background and design of the cloud and radiation test bed, *Bull. Am.. Meteorol. Soc.*, *75*, 1201–1221.

Turner, D. D. (2005), Arctic mixed-phase cloud properties from AERI-lidar observations: Algorithm and results from SHEBA, *J. Appl. Meteorol.*, *44*, 427–444.

Turner, D. D., and R. E. Holz (2005), Retrieving cloud fraction in the field-of-view of a high-spectral-resolution infrared radiometer, *Geosci. Remote Sens. Lett.*, *3*, 287–291, doi:10.1109/LGRS.2005.850533.

Turner, D. D., R. A. Ferrare, L. A. Heilman Brasseur, W. F. Feltz, and T. P. Tooman (2002), Automated retrievals of water vapor and aerosol profiles from an operational Raman lidar, *J. Atmos. Oceanic Technol.*, *19*, 37–50.

Turner, D. D., B. M. Lesht, S. A. Clough, J. C. Liljegren, H. E. Revercomb, and D. C. Tobin (2003a), Dry bias and variability in Vaisala radiosondes: The ARM experience, *J. Atmos. Oceanic Technol.*, *20*, 117–132.

Turner, D. D., S. A. Ackerman, B. A. Baum, H. E. Revercomb, and P. Yang (2003b), Cloud phase determination using ground-based AERI observations at SHEBA, *J. Appl. Meteorol.*, *42*, 701–715.

Turner, D. D., R. O. Knuteson, H. E. Revercomb, C. Lo, and R. G. Dedecker (2006), Noise reduction of atmospheric emitted radiance interferometer (AERI) observations using principal component analysis, *J. Atmos. Oceanic Technol.*, *23*, 1223–1238.

Turner, D. D., S. A. Clough, J. C. Liljegren, E. E. Clothiaux, K. Cady-Pereira, and K. L. Gaustad (2007a), Retrieving precipitable water vapor and liquid water path from Atmospheric Radiation Measurement (ARM) program's microwave radiometers, *IEEE Trans. Geosci. Remote Sens.*, in press.

Turner, D. D., et al. (2007b), Thin liquid water clouds: Their importance and our challenge, *Bull. Am. Meteorol. Soc.*, *88*, 177–190.

Westwater, E. R., Y. Han, M. D. Shupe, and S. Matrosov (2001), Analysis of integrated cloud liquid and precipitable water vapor retrievals from microwave radiometers during the Surface Heat Budget of the Arctic Ocean Project, *J. Geophys. Res.*, *106*, 32,019–32,030.

D. D. Turner, Space Science and Engineering Center, University of Wisconsin-Madison, 1225 West Dayton Street, Madison, WI 53706, USA. (dturner@ssec.wisc.edu)